Available online at www.sciencedirect.com
ScienceDirect
Optics Communications 266 (2006) 365–375
OPTICS COMMUNICATIONS
www.elsevier.com/locate/optcom

Optical properties of polarization-dependent geometric phase elements with partially polarized light

Yuri Gorodetski, Gabriel Biener, Avi Niv, Vladimir Kleiner, Erez Hasman *

Optical Engineering Laboratory, Faculty of Mechanical Engineering, Technion-Israel Institute of Technology, Technion City, Haifa 32000, Israel

Received 19 December 2005; received in revised form 23 March 2006; accepted 28 April 2006

Abstract

The behavior of geometric phase elements illuminated with partially polarized monochromatic beams is investigated both theoretically and experimentally. The element discussed in this paper is composed of wave plates with π-retardation and a space-variant orientation angle. We found that a beam emerging from such an element comprises two polarization orders; right-and left-handed circularly polarized states with conjugate geometric phase modification. This phase equals twice the orientation angle of the space-variant wave plate comprising the element. Apart from the two polarization orders, the emerging beam coherence polarization matrix includes a ''vectorial interference matrix'' which contains information concerning the correlation between the two orthogonal, circularly polarized portions of the incident beam. In this paper we measure this correlation by a simple interference experiment. In addition, we found that the equivalent mutual intensity of the emerging beam is modulated according to the geometric phase induced by the element. Other interesting phenomena concerning propagation will be discussed theoretically and demonstrated experimentally. The experiment made use of a spherical geometric phase element that was realized by use of a space-variant subwavelength grating illuminated with CO_2 laser radiation of 10.6 μm wavelength.

Keywords: Subwavelength gratings; Partial polarization; Polarization-dependent lens; Geometric phase

1. Introduction

When the polarization state of a beam traverses a close loop on the Poincaré sphere, the beam acquires a phase equal to half the area enclosed by the loop. This phase modification, which is described as a geometric phase, was investigated by Pancharatnam in the 1950s [1–3] and later on by Berry in the 1980s in the context of quantum systems [3,4]. Most of the papers which investigated the geometric phase considered the evolution of the phase over time [1–5]. The phase was initially generated by placing polarization elements, such as wave plates or polarizers, in sequence; the phase was then detected by the interference of the resulting beam with the incident beam. However, the polarization state of the manipulated beam is considered to be space-invariant. Geometric phase in the space domain has been theoretically investigated. Bhandari, for example, proposed the formation of a quadratic geometric phase by use of spatially rotating wave plates [6]. This phase was also demonstrated experimentally using different realization methods. Frins et al. and Zhen et al. proposed forming space-variant geometric phase elements by joining birefringent plates in different spatial orientations [7,8]. Such elements were also designed utilizing polarization recording media (e.g., bacteriorhodopsin) [9]. Recently, we proposed generating a geometric phase front based on a space-variant subwavelength dielectric grating [1,10–18]. Subwavelength gratings have opened new methods for forming beams with sophisticated phase and polarization distributions [19–21]. Using the above methods, elements with spatially varying wave plate orientations and of constant retardation were realized [22–24]. These elements form space-variant polarization state manipulation, which eventually leads to the geometric phase modification. Such elements are referred to as Pancharatnam–Berry phase optical

* Corresponding author. Tel.: +972 48292916; fax: +972 48295711.
E-mail address: mehasman@tx.technion.ac.il (E. Hasman).

0030-4018/$ - see front matter © 2006 Elsevier B.V. All rights reserved.
doi:10.1016/j.optcom.2006.04.044

elements (PBOEs). PBOEs have been exploited for near-field and far-field polarimetry [12,13], beam-splitting [14], encryption [15], polarization-dependant lenses [16], and have also been used in the formation of vectorial vortices [17,18]. In another application, space-domain geometric phase was used for nulling interferometry to detect a faint light source near a bright one [25].

The above mentioned studies were limited to the case of fully polarized illumination [1–11,14–18]. This naturally leads one to ask how a partially polarized beam behaves when transmitted through a geometric phase-induced element (PBOE), and what the propagation properties of this beam are when it emerges from such an element? Specifically, how do the intensity, the degree of polarization and the coherence of the beam depend on the transmission through the PBOE, and how are they affected afterwards on propagation through free space?

In this paper we investigate the optical properties of polarization-dependent geometric phase elements with partially polarized light. The analysis of a partially polarized monochromatic beam is performed using the beam coherence polarization (BCP) matrix formalism [13,26–28]. The ensuing propagation of the partially polarized beam in free space is analyzed by use of the extended van-Cittert Zernike integral [13,28]. By using the above formalism, we found that when a partially polarized beam is incident upon a π-retardation PBOE, the emerging beam comprises two polarization orders; right- and left-handed circularly polarized states with conjugate geometric phase modification. This phase equals twice the orientation angle of the space-variant wave plates comprising the PBOE. The intensity of the right (left)-handed circularly polarized order, RCP (LCP), equals the amount of the left (right)-handed circularly polarized portion of the incident beam. Apart from the BCPs of the two polarization orders, the emerging BCP comprises another matrix, which we term the ''vectorial interference matrix''. This matrix contains the information concerning the correlation between the RCP and LCP portions of the incident beam. The matrix distinguishes, for example, between an incident beam with a linearly polarized state versus an unpolarized state. In this paper we measure this correlation by transmitting the beam emerging from the PBOE through a polarizer-analyzer.

Furthermore, we find that while the intensity and degree of polarization are invariant upon transmission through a PBOE, the equivalent mutual intensity of the emerging beam is modulated according to the geometric phase induced by the PBOE. Other interesting phenomena regarding propagation will be discussed theoretically and experimentally demonstrated.

The theoretical analysis as well as the experimental results are investigated on a polarization-dependent PBOE lens. This lens focuses incoming light at different distances, depending on the polarization state as can be seen in Fig. 1(a) [16]. The intensities of the focal spots depend on the incident polarization state as will be shown experimentally for fully and partially polarized incident beams. The

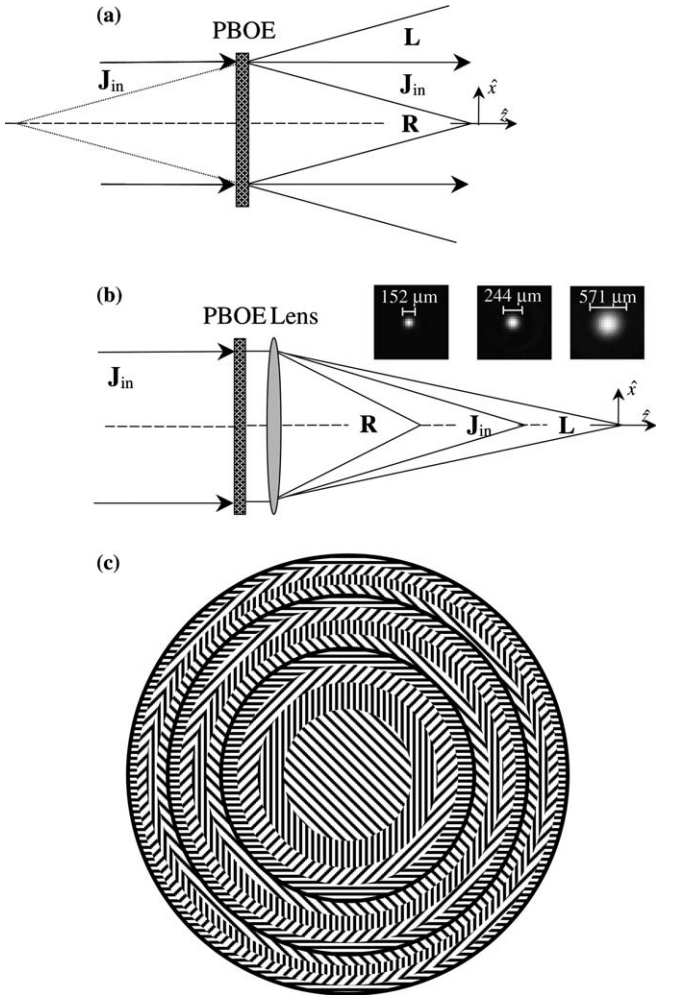

Fig. 1. Schematic presentation of a geometric phase element illuminated by a beam with a BCP matrix $\mathbf{J}_{in}$. The three emerging polarization orders are denoted by **L**, **R**, $\mathbf{J}_{in}$. (b) Concept of the multi-focal polarization-dependant lens achieved by combining the PBOE with a positive refractive lens. Insets show measured diffraction-limited spots for each focal plane. (c) Illustration of a magnified geometry of a PBOE lens mask with 4 discrete levels ($N = 4$).

analysis of partially polarized illumination upon a geometric phase element is elaborated in Section 2. In Section 3 we describe the design and realization procedures for a PBOE using space-variant subwavelength dielectric gratings. In Section 4 we present the experimental results for the geometric phase multi-focal lens achieved by a PBOE. Section 5 is devoted to concluding remarks.

2. Theoretical analysis

The analysis of partially polarized, quasi-monochromatic beams is conveniently performed by use of the BCP matrix calculus [13,26–28]. This formalism is derived from the more general case, the unified theory of coherence and polarization, which was developed by Wolf [29–34]. Assuming a beam propagating along the $\hat{z}$ axis, the 2×2 BCP matrix for a plane at constant z is defined as,

$$\mathbf{J}(\boldsymbol{\rho}_1,\boldsymbol{\rho}_2,z)=\begin{bmatrix} j^{\mathrm{RR}}(\boldsymbol{\rho}_1,\boldsymbol{\rho}_2,z) & j^{\mathrm{RL}}(\boldsymbol{\rho}_1,\boldsymbol{\rho}_2,z) \\ j^{\mathrm{LR}}(\boldsymbol{\rho}_1,\boldsymbol{\rho}_2,z) & j^{\mathrm{LL}}(\boldsymbol{\rho}_1,\boldsymbol{\rho}_2,z)\end{bmatrix}, \tag{1}$$

where $j^{\alpha\beta}(\boldsymbol{\rho}_1,\boldsymbol{\rho}_2,z)=\langle E^{*}_{\alpha}(\boldsymbol{\rho}_1,z)E_{\beta}(\boldsymbol{\rho}_2,z)\rangle$, $\alpha,\ \beta=R,\ L$ and $\boldsymbol{\rho}_1$, $\boldsymbol{\rho}_2$ are the transverse position vectors. The angle brackets denote time average, $E_{\alpha}(\boldsymbol{\rho},z)$ is the helical basis component of the electric field, and R and L denote the RCP and LCP states, respectively. The intensity of the beam, I, and the degree of polarization (DOP), P, can be calculated directly from this matrix [13,26–28,30–34]:

$$\begin{aligned} I(\boldsymbol{\rho},z)&=\mathrm{tr}\{\mathbf{J}(\boldsymbol{\rho},\boldsymbol{\rho},z)\},\\ P(\boldsymbol{\rho},z)&=\sqrt{1-\frac{4\det\{\mathbf{J}(\boldsymbol{\rho},\boldsymbol{\rho},z)\}}{[\mathrm{tr}\{\mathbf{J}(\boldsymbol{\rho},\boldsymbol{\rho},z)\}]^2}},\end{aligned} \tag{2}$$

where tr{} and det{} are the trace and the determinant of the matrix within the curl brackets. The DOP represents the ratio of the intensity of the polarized fraction's beam to the total intensity. It ranges from 1, when the beam is fully polarized, to 0 when the beam is unpolarized. We are interested in investigating beams emerging from a PBOE that are partially polarized.

PBOE is a rotating wave plate with a constant retardation ϕ, and a space-variant orientation function, $\theta(\boldsymbol{\rho})$. The transmission Jones matrix of a non-absorbing, non-scattering PBOE is given by

$$\begin{aligned}\mathbf{T}=\exp(\mathrm{i}\phi/2)\Bigg(&\cos(\phi/2)\begin{pmatrix}1&0\\0&1\end{pmatrix}\\ &-\mathrm{i}\sin(\phi/2)\begin{Bmatrix}0&\exp[\mathrm{i}2\theta(\boldsymbol{\rho})]\\ \exp[-\mathrm{i}2\theta(\boldsymbol{\rho})]&0\end{Bmatrix}\Bigg).\end{aligned} \tag{3}$$

The calculation of this transmission matrix is given in Appendix A. When a partially polarized beam is incident on the PBOE, the BCP matrix of the emerging beam is calculated as [13,26–28]

$$\mathbf{J}_{\mathrm{out}}(\boldsymbol{\rho}_1,\boldsymbol{\rho}_2,z=0)=\mathbf{T}^{+}(\boldsymbol{\rho}_1)\mathbf{J}_{\mathrm{in}}\mathbf{T}(\boldsymbol{\rho}_2), \tag{4}$$

where $\mathbf{J}_{\mathrm{in}}$ is the incident BCP matrix defined by Eq. (1). By substituting the Jones matrix from Eq. (3) into Eq. (4), the emerging BCP matrix obtained is

$$\begin{aligned}\mathbf{J}_{\mathrm{out}}=\eta_0\mathbf{J}_{\mathrm{in}}&+\eta_1 j^{\mathrm{LL}}\mathrm{e}^{\{2\mathrm{i}[\theta(\boldsymbol{\rho}_1)-\theta(\boldsymbol{\rho}_2)]\}}\mathbf{R}\\ &+\eta_1 j^{\mathrm{RR}}\mathrm{e}^{\{-2\mathrm{i}[\theta(\boldsymbol{\rho}_1)-\theta(\boldsymbol{\rho}_2)]\}}\mathbf{L}+\boldsymbol{\Gamma},\end{aligned} \tag{5}$$

where $\eta_0=\cos^2(\phi/2)$, $\eta_1=\sin^2(\phi/2)$ and $\mathbf{R}=\begin{pmatrix}1&0\\0&0\end{pmatrix}$, $\mathbf{L}=\begin{pmatrix}0&0\\0&1\end{pmatrix}$ are the BCP matrices for RCP and LCP states, and the matrix, $\boldsymbol{\Gamma}$, is provided in Appendix B. From Eq. (5) it is evident that the emerging BCP matrix comprises three polarization orders. The first order maintains the BCP matrix of the incident beam, the second order is a RCP beam with a space-variant phase modification, whereas the third order has a polarization direction and spatial phase dependence opposite in sign to that of the second one. The efficiency of the polarization orders depends on the PBOE transmission properties (η_0,η_1) and on the incident polarization state $(j^{\mathrm{LL}},j^{\mathrm{RR}})$. Apart from the three orders, the emerging BCP matrix in Eq. (5) also comprises a matrix denoted by $\boldsymbol{\Gamma}$. This matrix, which we denote as the vectorial interference matrix, contains the information about the correlation between the right and left-handed circularly polarized components of the incident beam. The matrix $\boldsymbol{\Gamma}$ and its properties are discussed in Appendix B. We choose to limit our discussion to a PBOE having retardation $\phi=\pi$. In this case $\eta_0=0$, $\eta_1=1$ and Eq. (5) degenerates to,

$$\mathbf{J}_{\mathrm{out}}=j^{\mathrm{LL}}\mathrm{e}^{\{2\mathrm{i}[\theta(\boldsymbol{\rho}_1)-\theta(\boldsymbol{\rho}_2)]\}}\mathbf{R}+j^{\mathrm{RR}}\mathrm{e}^{\{-2\mathrm{i}[\theta(\boldsymbol{\rho}_1)-\theta(\boldsymbol{\rho}_2)]\}}\mathbf{L}+\boldsymbol{\Gamma}_{\pi}, \tag{6}$$

where $\boldsymbol{\Gamma}_{\pi}$ is given by (see Appendix B),

$$\boldsymbol{\Gamma}_{\pi}=\begin{pmatrix}0&j^{\mathrm{LR}}\mathrm{e}^{\mathrm{i}2\theta[(\boldsymbol{\rho}_1)+\theta(\boldsymbol{\rho}_2)]}\\ j^{\mathrm{RL}}\mathrm{e}^{-\mathrm{i}2\theta[(\boldsymbol{\rho}_1)+\theta(\boldsymbol{\rho}_2)]}&0\end{pmatrix}. \tag{7}$$

It is evident from Eq. (6) that the first polarization order disappears and the above expression then comprises only two polarization orders with the corresponding phase modification. As this phase is created by a polarization manipulation by the element, it is geometric in nature [1,2]. To confirm this, we introduce the specific case of a plane wave with a RCP state (i.e., $\mathbf{J}_{\mathrm{in}}=\mathbf{R}$) incident on our PBOE. For such illumination, the matrix $\boldsymbol{\Gamma}_{\pi}$ is zero, and the resulting BCP is

$$\mathbf{J}_{\mathrm{out}}=\exp\{-2\mathrm{i}[\theta(\boldsymbol{\rho}_1)-\theta(\boldsymbol{\rho}_2)]\}\mathbf{L}. \tag{8}$$

In this case, the polarization of the incident beam is subjected to complete polarization state conversion, i.e., the right-handed circularly polarized incident beam becomes a left-handed circularly polarized. An important feature of Eq. (8) is the added phase factor, $2[\theta(\boldsymbol{\rho}_1)-\theta(\boldsymbol{\rho}_2)]$, that is determined by the difference between two local orientations of the rotating wave plate composing the PBOE. This dependence originates solely from the local changes in the polarization state of the emerging beam. In order to verify this dependence, we choose to employ the Poincaré sphere presentation. The Poincaré sphere is a unit sphere with the Stokes parameters S_1, S_2 and S_3 as its three axes (see Fig. 2) [35]. In this presentation, a polarization state can be mapped to a specific point on the sphere [1–6,10,11], whereas polarization state manipulation is represented by a path connecting the initial and final polarization states (points). When the polarization state of a beam traverses a close loop on the Poincaré sphere, a phase that equals half of the enclosed area is added to the beam [35]. Therefore, this phase can be regarded as a geometric phase [1,2,6,10,11]. In the described example, the polarization state of the emerging beam at two distinct points on the element travel along two geodesic lines, as depicted in Fig. 2. The separation of these lines equals the angle difference between the wave plates' orientations at these two points. Particularly for polarization state changes at $\boldsymbol{\rho}_1$ and $\boldsymbol{\rho}_2$, the angular separation of the related geodesic lines and consequently, half the area enclosed by them will be $2[\theta(\boldsymbol{\rho}_1)-\theta(\boldsymbol{\rho}_2)]$, which is exactly the phase modification as described in Eq. (8). The relation between the enclosed area and the angular separation can be derived by simple

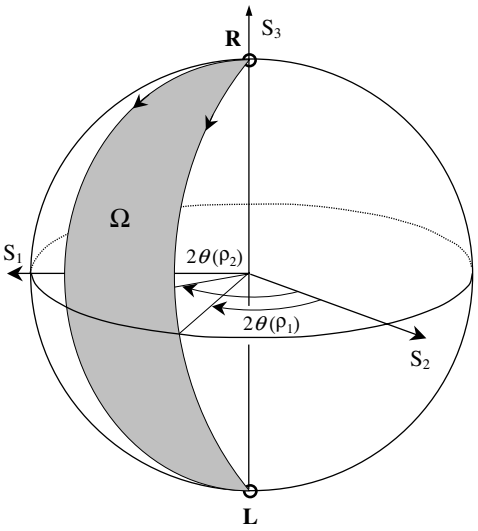

Fig. 2. Illustration of the principle of PBOEs using a Poincaré sphere.

geometric calculations [35]. Note that the geometric phase is not dependent on the incident wavelength. Illuminating the same element with $\mathbf{J}_{\text{in}} = \mathbf{L}$ will result in a RCP emerging beam with a phase modification opposite in sign to the one written in Eq. (8).

The above discussion regarding the geometric phase considers two specific cases of fully polarized light. However, we need to know how unpolarized light behaves when transmitted through a geometric phase element. In this case, $\mathbf{J}_{\text{in}}$ is a unit matrix, and the emerging BCP matrix is calculated from Eq. (6) to yield,

$$\mathbf{J}_{\text{out}}^{\text{UNP}} = \mathrm{e}^{\{2\mathrm{i}[\theta(\boldsymbol{\rho}_1)-\theta(\boldsymbol{\rho}_2)]\}}\mathbf{R} + \mathrm{e}^{\{-2\mathrm{i}[\theta(\boldsymbol{\rho}_1)-\theta(\boldsymbol{\rho}_2)]\}}\mathbf{L}. \tag{9}$$

Note that the polarization orders **R** and **L** result in equal efficiencies and conjugate geometric phase modifications. It is known that the unpolarized light can be generated by combining two uncorrelated beams with any orthogonal polarization states. However, the above outcome indicates that the PBOE acts on an unpolarized incident paraxial beam as if it were an incoherent superposition of RCP and LCP beams particularly. The general case of partially polarized beam with intensity I (see Eq. (2)) can be represented as a weighted sum of fully polarized and unpolarized light [35], i.e.,

$$\mathbf{J}_{\text{in}} = \frac{I}{2}[P\mathbf{J}_{\text{in}}^{\text{P}} + (1-P)\mathbf{J}_{\text{in}}^{\text{UNP}}], \tag{10}$$

where $\mathbf{J}_{\text{in}}^{\text{UNP}} = \begin{bmatrix} 1 & 0 \\ 0 & 1 \end{bmatrix}$ is the unpolarized fraction of the beam, $\mathbf{J}_{\text{in}}^{\text{P}} = \begin{bmatrix} j_{\text{P}}^{\text{RR}} & j_{\text{P}}^{\text{RL}} \\ j_{\text{P}}^{\text{LR}} & j_{\text{P}}^{\text{LL}} \end{bmatrix}$ is denoted as the polarized fraction, and,

$$j_{\text{P}}^{\alpha\beta} = \begin{cases} \frac{2}{I\cdot P} j^{\alpha\beta} & \text{for } \alpha \neq \beta, \\ \frac{2}{I\cdot P} j^{\alpha\beta} - \frac{1-P}{P} & \text{for } \alpha = \beta. \end{cases} \tag{11}$$

The BCP of the beam immediately after the element can be also decomposed into its polarized and unpolarized fractions. It can be shown that by applying $\mathbf{J}_{\text{in}}^{\text{P}}$ and $\mathbf{J}_{\text{in}}^{\text{UNP}}$ separately into Eq. (6), result in $\mathbf{J}_{\text{out}}^{\text{P}}$ and $\mathbf{J}_{\text{out}}^{\text{UNP}}$, which are the polarized and the unpolarized fractions of the emerging beam. Therefore, the transmission of each fraction through the element can be treated separately, i.e. the PBOE is a linear system as expected. The resulting BCP will have the form of,

$$\mathbf{J}_{\text{out}} = \frac{I}{2}[P\mathbf{J}_{\text{out}}^{\text{P}} + (1-P)\mathbf{J}_{\text{out}}^{\text{UNP}}], \tag{12}$$

where the BCP of the polarized fraction is given by,

$$\mathbf{J}_{\text{out}}^{\text{P}} = j_{\text{P}}^{\text{LL}}\mathrm{e}^{\{2\mathrm{i}[\theta(\boldsymbol{\rho}_1)-\theta(\boldsymbol{\rho}_2)]\}}\mathbf{R} + j_{\text{P}}^{\text{RR}}\mathrm{e}^{\{-2\mathrm{i}[\theta(\boldsymbol{\rho}_1)-\theta(\boldsymbol{\rho}_2)]\}}\mathbf{L} + \frac{2}{I\cdot P}\boldsymbol{\Gamma}. \tag{13}$$

This result indicates that the polarized fraction of a beam is divided into polarization orders according to its RCP and LCP components, as can be seen from Eq. (13), and acquires conjugate geometric phase modifications. However, the unpolarized fraction is equally divided into RCP and LCP states with the appropriate geometric phases (see Eq. (9)).

Calculating the DOP and the intensity of a beam emerging from a π-retardation PBOE is carried out using Eq. (2). From this equation we find that these properties are equal to those of the incident beam, as was expected. This result is obvious when considering a non-polarizing and non-absorbing element. Another physical property which can be studied is the equivalent mutual intensity [26,27,30,31], μ. This property can be obtained from a Young interference experiment (see Fig. 3) and is calculated from the BCP matrix of the beam as,

$$\mu(\boldsymbol{\rho}_1, \boldsymbol{\rho}_2, z) = \frac{\mathrm{tr}\{\mathbf{J}(\boldsymbol{\rho}_1, \boldsymbol{\rho}_2, z)\}}{[\mathrm{tr}\{\mathbf{J}(\boldsymbol{\rho}_1, \boldsymbol{\rho}_1, z)\}\mathrm{tr}\{\mathbf{J}(\boldsymbol{\rho}_2, \boldsymbol{\rho}_2, z)\}]^{1/2}}. \tag{14}$$

The absolute value of this quantity is proportional to the fringe visibility resulting from the experiment; hence, it becomes unity when the visibility is maximal and zero when the fringes disappear. The equivalent mutual intensity as calculated in Eq. (14) for partially polarized plane wave illumination results in,

$$\mu = A\exp(\mathrm{i}\psi), \tag{15a}$$

where

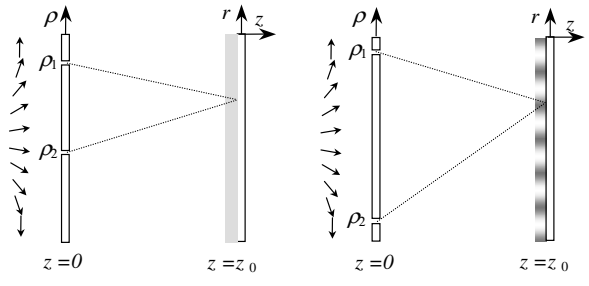

Fig. 3. Illustration of the Young interference experiment for a space-variant polarization field. The visibility of the fringes varies as a function of the two points selected in the transverse plane.

$$A=\sqrt{(j^{RR})^2+(j^{LL})^2+2j^{RR}j^{LL}\cos[4\theta(\boldsymbol{\rho}_1)-4\theta(\boldsymbol{\rho}_2)]}, \quad (15b)$$

and

$$\psi = a\tan\left\{\frac{j^{RR}-j^{LL}}{j^{RR}+j^{LL}}\tan[2\theta(\boldsymbol{\rho}_1)-2\theta(\boldsymbol{\rho}_2)]\right\}. \quad (15c)$$

As can be seen from Eq. (15), in contrast to the DOP and the intensity, the normalized equivalent mutual intensity, μ, is not conserved upon transmission. For example, unpolarized or partially polarized light in which the polarized fraction is in a linear state will result in,

$$\mu(\boldsymbol{\rho}_1,\boldsymbol{\rho}_2,z)=\cos[2\theta(\boldsymbol{\rho}_1)-2\theta(\boldsymbol{\rho}_2)]. \quad (16)$$

From Eq. (16) we see that the equivalent mutual intensity is a cosine function of the distance between two chosen points. This observation is not intuitive when considering transmission through a non-absorbing non-scattering element. Nevertheless, this phenomenon can be explained straightforwardly when conducting a Young interference experiment with a spatially varying polarized beam. Thus, as shown in Fig. 3, the interference of two points on the transverse plane with orthogonal polarization states, although totally correlated, will result in zero fringe visibility. On the other hand, two points with the same polarization state will result in maximum fringe visibility. Another interesting example would be the illumination of the π-retardation PBOE with a fully circularly polarized beam. In this case μ is given by

$$\mu(\boldsymbol{\rho}_1,\boldsymbol{\rho}_2,z)=\exp[i2\theta(\boldsymbol{\rho}_1)-i2\theta(\boldsymbol{\rho}_2)]. \quad (17)$$

Eq. (17) indicates that the visibility of the fringes is always maximal while their position depends on the distance of the two points chosen for the Young experiment. In the general case of partially polarized illumination, μ will have both amplitude and phase oscillations. This means that the visibility and the position of the fringes resulting from the Young interference experiment will depend on the choice of the distance between the two points. Note that the equivalent mutual intensity in both cases is being modulated according to the geometric phase of the element.

Up to this point we have analyzed the properties of the beam in the plane immediately after the element. However, we are also interested in investigating the above properties throughout propagation. The propagation of a partially polarized beam's BCP matrix in a linear and isotropic media is performed using the extended van-Cittert Zernike theorem [13,28]. Thus, the resulting BCP matrix elements are given by,

$$j_z^{\alpha\beta}(\mathbf{r}_1,\mathbf{r}_2,z)=\int_{-\infty}^{\infty} j_{out}^{\alpha\beta}(\boldsymbol{\rho}_1,\boldsymbol{\rho}_2,0)K^*(\mathbf{r}_1,\boldsymbol{\rho}_1,z)K(\mathbf{r}_2,\boldsymbol{\rho}_2,z)d^2\rho_1 d^2\rho_2, \quad (18)$$

where α and β equal R or L and $K(\mathbf{r},\boldsymbol{\rho},z)=\frac{-i\exp(ikz)}{\lambda}z\exp\left[\frac{ik}{2z}(\mathbf{r}-\boldsymbol{\rho})^2\right]$ is the paraxial propagation kernel. $k=2\pi/\lambda$ is the wavenumber and $\mathbf{r}$ is the transverse position vector in the output plane. The intensity at the distance z is calculated by tracing the resulting BCP matrix (see Eq. (2)). Therefore the intensity distribution of the propagating beam is given by,

$$I(\mathbf{r},z)=\frac{1}{(\lambda z)^2}\left[\int_{-\infty}^{\infty}[j^{LL}e^{2i[\theta(\boldsymbol{\rho}_1)-\theta(\boldsymbol{\rho}_2)]}+j^{RR}e^{-2i[\theta(\boldsymbol{\rho}_1)-\theta(\boldsymbol{\rho}_2)]}]\times e^{\frac{ik(\rho_2^2-\rho_1^2)}{2z}}K_{f1}^*K_{f2}d^2\rho_1 d^2\rho_2\right]_{\mathbf{r}_2=\mathbf{r}_1}, \quad (19)$$

where $K_{f_i}(\mathbf{r}_i,\boldsymbol{\rho}_i)=\exp\left[-\frac{ik}{z}(\mathbf{r}_i\cdot\boldsymbol{\rho}_i)\right]$ and $i=1,2$. Note that the expression in the square brackets is the sum of two intensity terms which correspond to the polarization order terms found in Eq. (6). As is evident from Eq. (7), the diagonal elements of matrix $\boldsymbol{\Gamma}_\pi$ are zero; therefore, none of the $\boldsymbol{\Gamma}_\pi$ matrix elements is apparent in Eq. (19). For the same reason we can expect that this matrix will not influence the equivalent mutual intensity of the propagating beam. This, however, will not be true for propagation in a polarization-dependant media such as uniaxial crystals or polarizers in which a coupling between the BCP matrix elements takes place.

To demonstrate our analysis of the propagation of partially polarized light, illuminating a geometric phase element, we chose a PBOE with a quadratic wave plate orientation function, i.e.,

$$\theta(\boldsymbol{\rho})=\left.\frac{\pi\boldsymbol{\rho}^2}{2\lambda f}\right|_{\mathrm{mod}\ 2pi}, \quad (20)$$

where f is the focal length and λ is the wavelength. Substituting Eq. (20) into Eq. (19) leads to cancellation of the quadratic phase factor of the first term for $z=f$ and of the second term for $z=-f$. Thus, for the case of the RCP plane wave illumination, the intensity at $z=f$ is found to be,

$$I(\mathbf{r}_1,\mathbf{r}_2,f)=\frac{1}{(\lambda f)^2}\delta(\mathbf{r}_1)\delta(\mathbf{r}_2), \quad (21)$$

where δ is the Dirac delta function. Hence, this element acts like a converging lens for RCP light. Using the same equation for a LCP incident beam results in diverging lens behavior. In the case of a finite aperture, the output intensity distribution will be calculated from the convolution of the far-field with the Fourier transform of the aperture function.

The focal plane of the PBOE lens is of special interest when considering the equivalent mutual intensity and the degree of polarization of the beam. The calculation of the BCP matrix in this plane is done by substituting Eq. (6) into Eq. (18) using the quadratic geometric phase written in Eq. (20). The resulting DOP, which is calculated by Eq. (2) from this BCP matrix equals unity throughout the focal plane ($z=f$). Similarly, the amplitude of the equivalent mutual intensity equals unity for every pair of points on this plane excluding the point $\mathbf{r}=0$. The results are the same regardless of the polarization state of the incident beam. These results are remarkable if one keeps in mind that the equivalent mutual intensity in the plane immediately after the PBOE lens is space-variant, as indicated by Eqs. (15)–

(17). The explanation of this phenomenon is contained in the BCP matrix resulting from Eq. (18). The calculations show that the beam is split into both a converging RCP and diverging LCP- state beam for any incident polarization state. The converging beam is focused in a spot that leaves the area of the focal plane illuminated by a coherent fully polarized LCP beam. This splitting yields a plane of fully polarized light with an equivalent mutual intensity of unit amplitude.

3. Design and realization of the PBOE lens

PBOEs can be realized by use of space-variant subwavelength dielectric gratings. When the period of the grating is much smaller than the incident wavelength, the grating behaves as a uniaxial crystal [1,36]. Therefore, we can form any desired PBOE by correctly determining the depth, structure, and orientation of the grating. Our objective is to design an element that when illuminated with a circularly polarized beam produces a spherical geometric phase distribution. The PBOE is required to add a phase, φ_d, which is given by,

$$\varphi_d = 2\theta = \frac{2\pi}{\lambda}\left(\sqrt{|\boldsymbol{\rho}|^2 + f^2}\right). \tag{22}$$

In our approach, a continuous desired phase function, $\varphi_d(\boldsymbol{\rho})$, is approximated by using discrete steps. The connection between the desired phase function and the discrete orientation function is given by

$$\theta(x,y)|_{\text{modpi}} = -F_N(\varphi_d(x,y))/2, \tag{23}$$

where $F_N()$ denotes a process that divides the desired phase, φ_d, into N equal levels. This division process is depicted in Fig. 4(a). In the scalar approximation an incident beam is multiplied by the phase function of the discrete phase element resulting in diffraction of the emerging beam. Quantification of this diffraction is obtained by Fourier expansion of the actual phase,

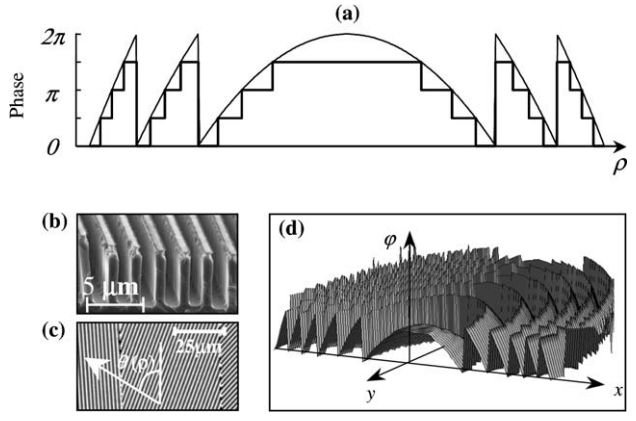

Fig. 4. (a) Illustration of the discrete phase of a PBOE with $N = 4$. (b and c) Scanning electron microscope (SEM) images taken from a small region of a PBOE lens that was realized on GaAs wafer. Note the rectangular shape of the subwavelength grooves and the space-variant groove orientation. (d) Measured phase of the emerging beam.

$$\exp(iF_N(\varphi_d)) = \sum_m C_m \exp(im\varphi_d), \tag{24}$$

where C_m is the mth order coefficient of the Fourier expansion. The diffraction efficiency of the mth diffracted order is given by $|C_m|^2$. The first diffraction order represents an exact replica of the desired phase, φ_d. Consequently, the diffraction efficiency, $|C_1|^2$, for the first diffracted order is related to the number of discrete levels N by

$$|C_1|^2 = \left[\frac{N}{\pi}\sin\left(\frac{\pi}{N}\right)\right]^2. \tag{25}$$

This equation indicates that for 2, 4, 8, and 16 discrete phase levels, the diffraction efficiency will be 40.5%, 81.1%, 95.0%, and 98.7%, respectively. The connection between the first order diffraction efficiency and the number of discrete levels was verified experimentally in Refs. [1,16].

We formed a binary chrome mask using high-resolution laser lithography. The amplitude transmission, $t(x,y)$, of the mask is derived from

$$t(x,y) = U_s\left[\cos\left(\frac{2\pi}{\Lambda}(x\cos\theta(x,y) + y\sin\theta(x,y))\right) - \cos(\pi q)\right], \tag{26}$$

where Λ and q are the period and fill factor of the subwavelength grating, respectively, x, y are the transverse plane Cartesian coordinates, and U_s is the unit step function defined by

$$U_s(\xi) = \begin{cases} 1, & \xi \geqslant 0, \\ 0, & \xi < 0. \end{cases} \tag{27}$$

The mask was 10 mm in diameter and $\theta(x,y)$ was calculated from Eqs. (22) and (23) where $\lambda = 10.6$ μm, $f = 200$ mm and the number of discrete levels $N = 8$. According to Eq. (25), we expected to obtain more than a 94% diffraction efficiency into the first order. A subwavelength period of $\Lambda = 2$ μm was selected together with a fill factor $q = 0.5$ for use with CO_2 laser radiation of a 10.6 μm wavelength. Fig. 1(c) shows a magnified geometry of the mask. The mask was transferred by contact lithography to 500 μm- thick GaAs wafers onto which had been predeposited a 2000 Å layer of SiN_x. The SiN_x deposition was achieved by enhanced chemical vapor deposition (PECVD) at 900 mTorr and 300 °C. At this stage, a 700 Å Ni adhesion layer was used for the lift-off process. Next, the SiN_x layer was etched through the Ni strips, which served as a mask. The etching was performed by reactive ion etching (RIE – Plasma-Therm 790) for 30 s at room temperature with CF_4 and O_2 at gas flow rates of 35 sccm and 14 sccm, respectively, and at a pressure of 80 mTorr. The GaAs was then etched by electron cyclone resonance (ECR – Plasma-Therm SLR) for about eight minutes, with the etched SiN_x layer serving as a mask. The ECR conditions were: 20 sccm of Cl_2, 5 sccm of Ar, 75 W RF power and 600 W microwave power, at 100 °C. The remaining SiN_x was removed using HF acid resulting in a grating of 5 μm nominal depth for a $\phi = \pi$ retardation

element. The final step in fabricating the desired PBOE involved depositing an anti-reflection coating on the backside of the elements. Fig. 4(b) and (c) shows scanning electron microscope (SEM) images of a small area of the $\phi = \pi$ element. Note the high aspect ratio ($\sim$1/5) and the rectangular shape of the grooves. In order to confirm the formation of the desired phase, we used an experimental procedure described in Section 4 of Ref. [17]. The measured geometric phase added by the PBOE is presented in Fig. 4(d). The transmission coefficients of the PBOEs were also measured and resulted in $t_x = 0.96$ and $t_y = 0.94$ for light polarized parallel and perpendicular to the grating grooves respectively, while the retardation of the element was found to be $\phi = 0.9\pi$. The measured values were close to the theoretical predictions of $t_x = 0.959$, $t_y = 0.936$ and $\phi = \pi$, obtained by using rigorous coupled wave analysis.

4. Experimental results

In order to investigate the behavior of the element with partially polarized illumination, we formed an incident beam by combining two orthogonally polarized CO_2 laser beams with a polarizing beam combiner (see Fig. 5(a)). The resultant DOP, as calculated by Eq. (2), is given by

$$P = \left|\frac{I_2 - I_1}{I_1 + I_2}\right|, \tag{28}$$

where I_1 and I_2 are the intensities of the lasers. By setting one of the lasers' intensities to zero, a fully polarized beam was achieved. To produce unpolarized light we used laser beams with equal intensities, i.e., $I_1 = I_2$. First, we tested the correlation between the RCP and the LCP portions of the incident beam. This correlation is expressed by the off-diagonal elements of the vectorial interference matrix, $\mathbf{\Gamma}$, and can be measured by placing a linear analyzer-polarizer behind the PBOE. The use of an analyzer imposes a coupling between the BCP matrix elements of the beam emerging from the PBOE, as can be seen in the calculations included in Appendix B. The intensity distribution behind a π-retardation PBOE followed by the analyzer, illuminated with a plane-wave of partial polarization is calculated using Eq. (B.3) and yields,

$$I_p = \frac{1}{2} I_{in} + |j^{RL}| \cos[4\theta(\boldsymbol{\rho}) - \arg(j^{RL})]. \tag{29}$$

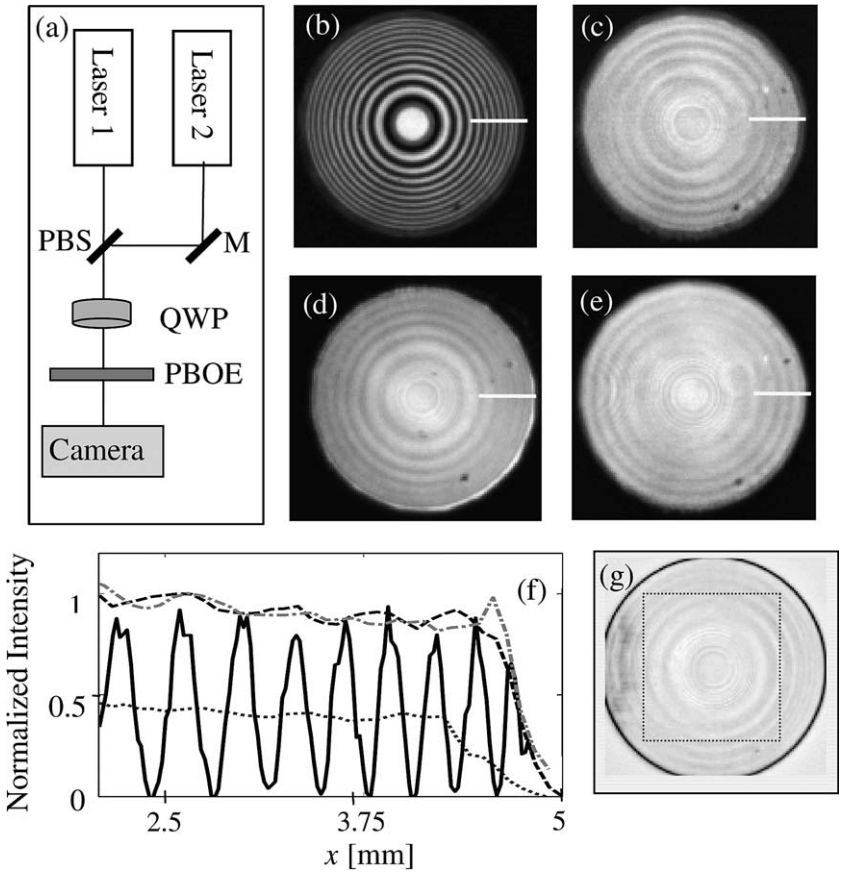

Fig. 5. (a) Setup for combining the two lasers to generate partially polarized light: PBS – a polarization beam-splitter, M – mirror. (b, c) Intensity distributions of the beam emerging from the PBOE followed by an analyzer with (b) linearly polarized illumination and (c) unpolarized illumination. (d,e) Intensity distribution of the beam emerging from the PBOE when illuminated by (d) linearly polarized light, (e) unpolarized light. (f) Normalized intensity distribution cross-sections measured, along the white line depicted in (b–e), for the unpolarized illumination (dashed line), unpolarized illumination with the polarizer (dotted line), linearly polarized illumination (dashed-doted line) and linearly polarized illumination with a polarizer (solid line). (g) Measured DOP distribution over the beam beyond the PBOE when illuminated by a circularly polarized light.

This equation makes evident the periodic behavior of the intensity with the inclusion of the mean value of $I_{in}/2$, and with a modulation equal to the absolute value of j^{RL}. More explicitly, when $|j^{RL}| = 1$, i.e., there is complete correlation between the RCP and LCP states and the visibility of the fringes is unity. This case is depicted in Fig. 5(b) in which the PBOE was illuminated by linearly polarized light, and the near-field intensity was captured by a Spiricon Pyrocam III camera. The high visibility of the fringes can be observed in this figure. However, when RCP and LCP portions of the incident beam are uncorrelated ($|j^{RL}| = 0$), the visibility of the fringes is zero. We demonstrated this case by illuminating the PBOE with unpolarized light. The resulting intensity distribution is presented in Fig. 5(c), in which no fringes are observed. Note that the combination of the PBOE with a linear analyzer can be exploited to measure the degree of correlation between the RCP and LCP components of a partially polarized beam. Next, the analyzer was removed, and the intensity distribution behind the element was captured. This result is presented in Fig. 5(d) for linearly polarized illumination and 5(e) for unpolarized illumination. No modulation can be seen in these figures, because the matrix $\mathbf{\Gamma}$ does not affect the intensity. To visualize the modulation depth of the mentioned intensity distributions, we present cross-sections of these measurements in Fig. 5(f). With the use of the analyzer, it can be clearly observed that the fully polarized incident beam results in a high intensity modulation, (typically of 0.9), but that when the element is illuminated with an unpolarized beam, very low intensity modulation is seen, (typically of 0.08). These values are close to the theoretical ones, which are 1 for the polarized illumination and 0 for the unpolarized illumination. We also measured the DOP in the plane behind the element illuminated by a RCP beam using a four-measurement technique [35]. This measurement is shown in Fig. 5(g) and demonstrates almost complete uniformity in the behavior of the DOP in the output plane. We have calculated the mean value of the DOP within the square area depicted in Fig. 5(g) to be 0.98 with standard deviation of 0.003 compared to 2% non-uniformity of the quarter wave plate (QWP) used for the measurement. These results prove that our PBOE is a non-polarizing element as required.

Section 2 provides the explanation for the dependence of a geometric phase induced by a PBOE on the incident polarization state. We devised the scheme depicted in Fig. 1(b) to experimentally confirm this dependence. For this purpose we used the element designed and realized in Section 3, i.e., a π-retardation spherical-phase PBOE. Our element acts as a polarization-dependant lens with a focal length $f = 200$ mm for RCP light and $-f$ for LCP light (see Fig. 1(a)). The third polarization order, $\mathbf{J}_{in}$, appears as a result of an etching error of the element which causes a deviation from the π-retardation. The appearance of this polarization order can be calculated from Eq. (5) using the measured retardation phase of $\phi = 0.9\pi$ to be $\eta_0 = 0.024$. To focus the three polarization orders along the positive direction of the z-axis, a refractive lens was inserted behind the element. The focal length of the refractive lens was $f_r = 127$ mm. The phase induced by the resulting composite element is the sum of the polarization-dependent geometric phase obtained by the PBOE and the dynamic phase obtained by the refractive lens. We illuminated the combined element with a linearly polarized light. A rotating QWP was used as a polarization state generator. Fig. 6 shows the measured and predicted efficiencies of the three polarization orders' intensities as a function of the QWP orientation angle. Three examples of such spots are shown in the insets of Fig. 1(b). These spots were experimentally found to be diffraction limited. The polarization orders denoted by **R**, **L** and $\mathbf{J}_{in}$ correspond to the three orders depicted in Fig. 1(b). As can be seen from Fig. 6, the efficiencies of the three polarization orders depend on the RCP and LCP portions in the incident beam. For example, when the PBOE is illuminated by RCP light, most of the beam intensity is being focused to the **L** plane according to Eq. (21). This example corresponds to the QWP orientation of 135° (see Fig. 6). From this figure it is evident that the intensity of the **L** polarization order is close to unity while the intensity of the **R** polarization orders is zero. Note the low efficiency of the $\mathbf{J}_{in}$ order which indicates that the analyzed PBOEs retardation is close to π. The curves of the **R** and the **L** orders coincide for a linearly polarized incident beam which is achieved by orienting the QWP at 90°. This figure indicates that our composite element behaves as a multi-focal polarization-dependent lens.

We also experimentally investigated the behavior of this element with partially polarized illumination. The DOP of the incident beam has been controlled by adjusting the intensity of one of the lasers while keeping the second one constant. We considered the superposition of two orthogonal linearly polarized as well as circularly polarized

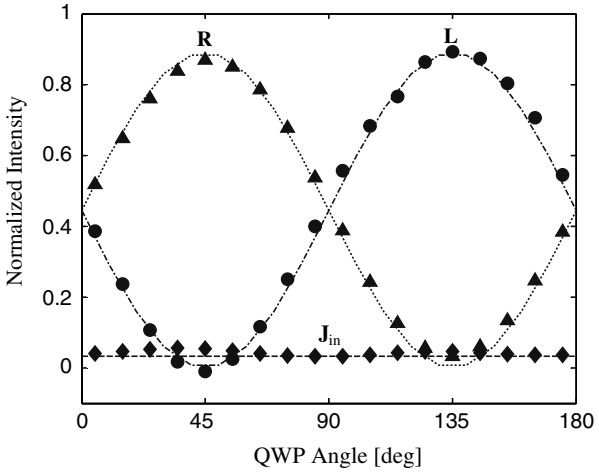

Fig. 6. Normalized intensity at different focuses of a composite element as a function of QWP orientation. Triangles are the measurements in the **R** focal plane, circles in the **L** focal plane and diamonds are the measurements in the focal plane of the $\mathbf{J}_{in}$ order. The dotted, dash-dotted and dashed lines are the theoretical calculations for each order respectively.

lasers. The BCP matrix for orthogonal linearly polarized uncorrelated beams combining is,

$$\mathbf{J}_{\text{in}} = \frac{(I_1 + I_2)}{2}\begin{bmatrix} 1 & P\cdot \text{sgn}(I_2 - I_1) \\ P\cdot \text{sgn}(I_2 - I_1) & 1 \end{bmatrix}, \quad (30)$$

where sgn is a sign function. The combining of two uncorrelated orthogonal circularly polarized beams is represented by the BCP matrix,

$$\mathbf{J}_{\text{in}} = \frac{I_1 + I_2}{2}\begin{bmatrix} 1 + P\cdot \text{sgn}(I_1 - I_2) & 0 \\ 0 & 1 - P\cdot \text{sgn}(I_1 - I_2) \end{bmatrix}. \quad (31)$$

Both types of combining were achieved by using the setup depicted in Fig. 5(a) with the QWP oriented at 0° and 45°, respectively. Fig. 7 describes the measured focal spot intensity in the **R** polarization order focal plane for both combining schemes as a function of intensity ratio I_1/I_2. As evident from Fig. 7, when the incident beam is composed of two orthogonal linearly polarized beams, the efficiencies of the **R** and **L** orders are equal regardless of the intensity ratio of the combined beams. However, when the beam is composed of two orthogonal circularly polarized beams, the polarization order efficiency becomes a function of the intensity ratio of the combined beams. For instance, when the intensity ratio is zero, i.e., the beam is in a LCP state, the **R** focal spot intensity will be maximal. On the other hand, for the infinite intensity ratio, i.e., when the incident beam is in a RCP state, the **R** order focal spot will yield zero intensity. Therefore, it is possible to modulate the polarization orders' efficiencies by controlling the intensity ratio of the uncorrelated beams combining in a circularly polarized state. The point where $I_1/I_2 = 1$ corresponds to the unpolarized beam ($P = 0$). At that point the two lines coincide, indicating similar behavior of the two combining beams.

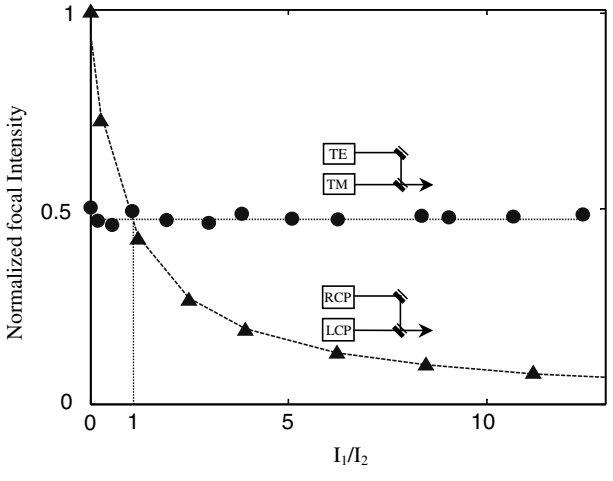

Fig. 7. Measured intensity at the focus of the RCP order as a function of the intensity ratio of two lasers. Circles indicate the measured intensity for partially polarized light with linearly polarized fraction. Triangles indicate the measured intensity for partially polarized light with circularly polarized fraction. Dotted and the dashed lines are the theoretical predictions for the above cases. Vertical dotted line illustrates a point with zero DOP.

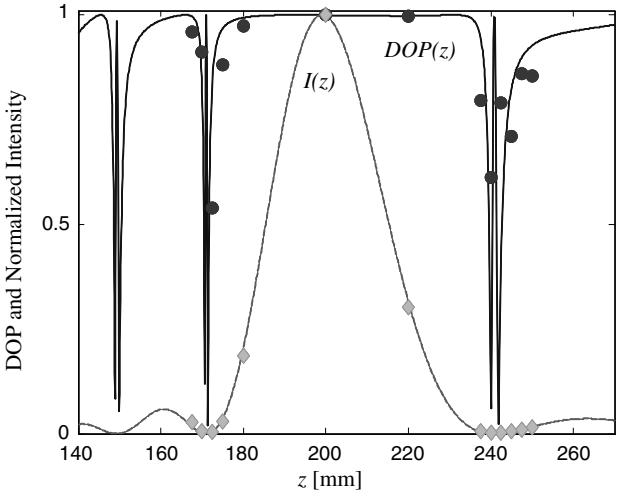

Fig. 8. Predicted and measured DOP and intensity on-axis distributions along z-axis in the vicinity of the **R** polarization order focus. Solid and dashed lines indicate the calculated DOP and the intensity respectively on the z-axis. Experimental measurements for the DOP and the intensity are plotted by circles and diamonds, respectively.

An interesting phenomenon concerning the propagation properties of the beam was observed when illuminating the PBOE with unpolarized light. The DOP along the z-axis was measured in the front focal region of the PBOE, (without the refractive lens). We can see that while the intensity is a sinc-like [37] function, the DOP is close to a rectangular shape within the focal depth, as can be seen in Fig. 8. This effect can be explained as follows: the two emerging polarization orders in this case are uncorrelated, hence the DOP along the axis can be found from Eq. (28), where I_1 and I_2 are replaced by the intensities of the polarization orders on the z-axis. These intensity distributions along the z-axis are of sinc-function form, however they are relatively shifted along the z-axis (the two focal distances $f = \pm 200$ mm). The zeros of the DOP depicted in Fig. 8 correspond to equal order intensities, while the high values of the DOP match the regions where one of the orders intensity is close to zero. This result indicates that the DOP is changed along propagation. The variation of the DOP along the propagation axis was investigated earlier [28,34,38]. However, in our case, it is possible to control the shape of the DOP along the propagation axis by choosing the focal length of a PBOE or alternatively choosing a PBOE with a sophisticated geometric phase [13].

5. Conclusion

The behavior of geometric phase elements (PBOEs) illuminated by partially polarized monochromatic beams was analyzed. We have shown that in the case of partially polarized illumination the beam emerging from a PBOE with a π-retardation comprises two polarization orders. The first and the second polarization orders are RCP and LCP states, respectively. Both polarization orders acquire conjugate geometric phase modifications that result from

a polarization state manipulation created by the element. The intensity of the RCP (LCP) polarization order is equal to the amount of the LCP (RCP) portion in the incident beam. Apart from the two polarization orders, the emerging BCP comprises a matrix termed the "vectorial interference matrix". This matrix contains the information concerning the correlation between the RCP and the LCP portions of the incident beam. We suggested a simple interference experiment to measure the degree of this correlation by placing a polarizer behind the PBOE and measuring the emerging intensity. We have shown experimentally that the vectorial interference matrix distinguishes between the cases of linearly polarized and unpolarized illumination. The PBOE used for the experimental demonstration was a spherical geometric phase PBOE designed for CO_2 laser radiation and realized on a GaAs wafer with a subwavelength grating. We have shown that this PBOE followed by a refractive lens behaves as a multi-focal polarization-dependent lens. Such a lens can be implemented in a variety of applications, such as multi-layer data storage and polarization imaging [39,24]. We also studied the intensity, the normalized equivalent mutual intensity, and the DOP immediately after the element and upon propagation in free-space. We found that the equivalent mutual intensity was modulated according to the geometric phase induced by the element. Moreover, we showed that in the focal plane of the PBOE lens, the DOP and the amplitude of the equivalent mutual intensity become unity regardless of the incident polarization state. This property can be used in applications such as a polarizer or a polarizing beam-splitter by placing a spatial filter in this plane.

Appendix A

A PBOE behaves as a space-variant wave plate element with constant retardation, ϕ, and a space-varying fast axis, $\theta(\boldsymbol{\rho})$, along the $\boldsymbol{\rho}$ coordinate [1,10,11,15–17]. The Jones matrix of such an element is written as,

$$\mathbf{T}_c = \mathbf{M}^{-1}(\theta)\mathbf{W}(\phi)\mathbf{M}(\theta), \tag{A.1}$$

where $\mathbf{M}$ and $\mathbf{W}$ represent the rotation matrix and the matrix of a non-polarizing wave plate oriented in the $\hat{\mathbf{x}}$ direction. Explicitly, these matrices are given by,

$$\mathbf{M} = \begin{pmatrix} \cos(\theta) & \sin(\theta) \\ -\sin(\theta) & \cos(\theta) \end{pmatrix}; \quad \mathbf{W} = \begin{pmatrix} 1 & 0 \\ 0 & \exp(\mathrm{i}\phi) \end{pmatrix}. \tag{A.2}$$

In the case of a PBOE, it is convenient to transform the Jones matrix to a helicity basis in which the vector bases are the right and left-handed circularly polarized states, i.e. $\mathbf{RCP} = (1 \quad 0)^{\mathrm{T}}$ and $\mathbf{LCP} = (0 \quad 1)^{\mathrm{T}}$. The conversion of $\mathbf{T}_c$ to the helicity basis results in a transmission matrix of

$$\mathbf{T} = \mathbf{U}^{-1}\mathbf{T}_c\mathbf{U}, \tag{A.3}$$

where $\mathbf{U}$ is the unitary transformation matrix, written as

$$\mathbf{U} = \frac{1}{\sqrt{2}}\begin{pmatrix} 1 & 1 \\ -i & i \end{pmatrix}. \tag{A.4}$$

Accordingly, the PBOE transmission matrix is written explicitly as,

$$\mathbf{T} = \exp(\mathrm{i}\phi/2)\left\{\cos(\phi/2)\begin{bmatrix} 1 & 0 \\ 0 & 1 \end{bmatrix} - \mathrm{i}\sin(\phi/2)\begin{bmatrix} 0 & \mathrm{e}^{\mathrm{i}2\theta(\boldsymbol{\rho})} \\ \mathrm{e}^{-\mathrm{i}2\theta(\boldsymbol{\rho})} & 0 \end{bmatrix}\right\}. \tag{A.5}$$

Appendix B

The expression for the BCP matrix emerging from a PBOE (Eq. (5)) contains a matrix denoted by $\boldsymbol{\Gamma}$. This matrix is defined as,

$$\boldsymbol{\Gamma} = \begin{pmatrix} \gamma_{1,1} & \gamma_{1,2} \\ \gamma_{2,1} & \gamma_{2,2} \end{pmatrix}, \tag{B.1}$$

where the $\boldsymbol{\Gamma}$ matrix elements are given by,

$$\begin{aligned} \gamma_{1,1} &= i\sqrt{\eta_0\eta_1}\left(j^{\mathrm{LR}}\mathrm{e}^{\mathrm{i}2\theta(\boldsymbol{\rho}_1)} - j^{\mathrm{RL}}\mathrm{e}^{-\mathrm{i}2\theta(\boldsymbol{\rho}_2)}\right), \\ \gamma_{1,2} &= i\sqrt{\eta_0\eta_1}\left(j^{\mathrm{LL}}\mathrm{e}^{\mathrm{i}2\theta(\boldsymbol{\rho}_1)} - j^{\mathrm{RR}}\mathrm{e}^{\mathrm{i}2\theta(\boldsymbol{\rho}_2)}\right) + \eta_1\left(j^{\mathrm{LR}}\mathrm{e}^{\mathrm{i}2\theta[(\boldsymbol{\rho}_1)+\theta(\boldsymbol{\rho}_2)]}\right), \\ \gamma_{2,1} &= i\sqrt{\eta_0\eta_1}\left(j^{\mathrm{RR}}\mathrm{e}^{-\mathrm{i}2\theta(\boldsymbol{\rho}_1)} - j^{\mathrm{LL}}\mathrm{e}^{-\mathrm{i}2\theta(\boldsymbol{\rho}_2)}\right) + \eta_1\left(j^{\mathrm{RL}}\mathrm{e}^{-\mathrm{i}2\theta[(\boldsymbol{\rho}_1)+\theta(\boldsymbol{\rho}_2)]}\right), \\ \gamma_{2,2} &= i\sqrt{\eta_0\eta_1}\left(j^{\mathrm{RL}}\mathrm{e}^{-\mathrm{i}2\theta(\boldsymbol{\rho}_1)} - j^{\mathrm{LR}}\mathrm{e}^{\mathrm{i}2\theta(\boldsymbol{\rho}_2)}\right). \end{aligned} \tag{B.2}$$

Note, that the trace of $\boldsymbol{\Gamma}$ is zero at $\boldsymbol{\rho}_1 = \boldsymbol{\rho}_2$, thus, the intensity of the emerging beam, presented by Eq. (5), is not affected by this matrix. However, the off-diagonal elements are of great importance since they bear the information on the correlation of the polarization components, i.e., j^{RL} and j^{LR}. One can measure the degree of correlation by transmitting the emerging beam through a polarizer. The calculation of the resulting intensity can be found from: $I_{\mathrm{p}} = \mathrm{tr}\{\mathbf{P}^{+}\mathbf{J}_{\mathrm{out}}\mathbf{P}\}$, where the transmission matrix of a polarizer is $\mathbf{P} = \frac{1}{2}\begin{pmatrix} 1 & 1 \\ 1 & 1 \end{pmatrix}$ and $\mathbf{J}_{\mathrm{out}}$ is the beam's BCP matrix as calculated by Eq. (5). The resulting intensity would be,

$$\begin{aligned} I_{\mathrm{p}} = {} & \frac{1}{2}I_{\mathrm{in}} + \cos^2\left(\frac{\phi}{2}\right)|j^{\mathrm{RL}}|\cos[\arg(j^{\mathrm{RL}})] \\ & + \sin^2\left(\frac{\phi}{2}\right)|j^{\mathrm{RL}}|\cos[4\theta(\boldsymbol{\rho}) - \arg(j^{\mathrm{RL}})] \\ & + \frac{1}{2}\sin\phi\sin 2\theta(j^{\mathrm{RR}} - j^{\mathrm{LL}}), \end{aligned} \tag{B.3}$$

where I_{in} is the incoming intensity. Note that I_{p} is modulated according to the off-diagonal elements of the $\boldsymbol{\Gamma}$ matrix, and thus, by Fourier analysis we can extract the correlation values, j^{RL} and j^{LR}.

References

[1] E. Hasman, G. Biener, A. Niv, V. Kleiner, Space-variant polarization manipulation, in: E. Wolf (Ed.), Progress in Optics, 47, Elsvier, Amsterdam, 2005.
[2] S. Pancharatnam, Proc. Ind. Acad. Sci. 44 (1956) 247.
[3] M.V. Berry, J. Mod. Opt. 34 (1987) 1401.

[4] M.V. Berry, Proc. Roy. Soc. London A 392 (1984) 45.
[5] R. Bhandari, J. Samuel, Phys. Rev. Lett. 60 (1988) 1211.
[6] R. Bhandari, Phys. Rep. 281 (1997) 1.
[7] E.M. Frins, J.A. Ferrari, A. Dubra, D. Perciante, Opt. Lett. 25 (2000) 284.
[8] Q. Zhan, J.R. Leger, Opt. Commun. 213 (2002) 241.
[9] J.A. Ferrari, E. Garbusi, E.M. Frins, Opt. Lett. 29 (2004) 1138.
[10] Z. Bomzon, V. Kleiner, E. Hasman, Opt. Lett. 26 (2001) 1424.
[11] Z. Bomzon, G. Biener, V. Kleiner, E. Hasman, Opt. Lett. 27 (2002) 1141.
[12] G. Biener, A. Niv, V. Kleiner, E. Hasman, J. Opt. Soc. Am. A 20 (2003) 1940.
[13] Y. Gorodetski, G. Biener, A. Niv, V. Kleiner, E. Hasman, Opt. Lett. 30 (2005) 2245.
[14] E. Hasman, Z. Bomzon, A. Niv, G. Biener, V. Kleiner, Opt. Commun 209 (2002) 45.
[15] G. Biener, A. Niv, V. Kleiner, E. Hasman, Opt Lett. 30 (2005) 1096.
[16] E. Hasman, V. Kleiner, G. Biener, A. Niv, Appl. Phys. Lett. 82 (2003) 328.
[17] A. Niv, G. Biener, V. Kleiner, E. Hasman, Opt. Commun. 251 (2005) 306.
[18] A. Niv, G. Biener, V. Kleiner, E. Hasman, Opt. Lett. 30 (2005) 2933.
[19] F. Xu, R.C. Tian, P.C. Sun, Y. Fainman, C.C. Cheng, A. Scherer, Opt. Lett. 20 (1995) 2457.
[20] F. Xu, R.C. Tian, P.C. Sun, Y. Fainman, C.C. Cheng, A. Scherer, Opt. Lett. 21 (1996) 1513.
[21] P. Lalanne, S. Astilean, P. Chavel, E. Cambril, H. Launois, J. Opt. Soc. Am. A 16 (1999) 1143.
[22] J. Tervo, J. Turunen, Opt. Lett. 25 (2000) 785.
[23] J. Tervo, V. Kettunen, M. Honkanen, J. Turunen, J. Opt. Soc. Am. A 20 (2003) 282.
[24] G.P. Nordin, J.T. Meier, P.C. Deguzman, M.W. Jones, J. Opt. Soc. Am. A 16 (1999) 1168.
[25] N. Baba, N. Murakami, T. Ishigaki, Opt. Lett. 26 (2001) 1167.
[26] F. Gori, Opt. Lett. 23 (1998) 241.
[27] F. Gori, M. Santarsiero, S. Vicalvi, R. Borghi, G. Guattari, Pure Appl. Opt. 7 (1998) 941.
[28] F. Gori, M. Santarsiero, R. Borghi, G. Piquero, Opt. Lett. 25 (2000) 1291.
[29] L. Mandel, E. Wolf, Optical Coherence and Quantum Optics, Cambridge University Press, USA, 1995.
[30] E. Wolf, Opt. Lett. 28 (2003) 1078.
[31] E. Wolf, Phys. Lett. A 312 (2003) 263.
[32] T. Shirai, E. Wolf, J. Opt. Soc. Am. A 21 (2004) 1907.
[33] G.S. Agarwal, A. Dogariu, T.D. Visser, E. Wolf, Opt. Lett. 30 (2005) 120.
[34] O. Korotkova, E. Wolf, Opt. Commun. 246 (2005) 35.
[35] C. Brosseau, Fundamentals of Polarized Light; A Statistical Optics Approach, John Wiley & Sons, USA, 1998.
[36] M. Born, E. Wolf, Principles of Optics, Cambridge University Press, UK, 1999.
[37] J.W. Goodman, Introduction to Fourier Optics, McGraw-Hill, Singapore, 1996.
[38] D.F.V. James, J. Opt. Soc. Am. A 11 (1994) 1641.
[39] K. Kinnstatter, M. Ojima, S. Yonezawa, Appl. Opt. 29 (1990) 4408.